Journal of Geoscience and Environment Protection, 2024, 12, 233-252
https://www.scirp.org/journal/gep
ISSN Online: 2327-4344
ISSN Print: 2327-4336

Parameterizing the Wind Friction Velocity and Characterization of Flow Regimes at Omu Creek, Mahin in Ilaje Local Government Area, Ondo State, Southwestern Nigeria

Adekunle Ayodotun Osinowo[1*], Lateef Adesola Afolabi[2], Pasquale Contestabile[2]

[1]Department of Marine Science and Technology, Federal University of Technology, Akure, Nigeria
[2]Department of Engineering, University of Campania Luigi Vanvitelli, Aversa, Italy
Email: *aaosinowo@gmail.com, lateefadesola.afolabi@unicampania.it, pasquale.contestabile@unicampania.it

How to cite this paper: Osinowo, A. A., Afolabi, L. A., & Contestabile, P. (2024). Parameterizing the Wind Friction Velocity and Characterization of Flow Regimes at Omu Creek, Mahin in Ilaje Local Government Area, Ondo State, Southwestern Nigeria. *Journal of Geoscience and Environment Protection, 12,* 233-252.
https://doi.org/10.4236/gep.2024.1212015

Received: November 12, 2024
Accepted: December 22, 2024
Published: December 25, 2024

Abstract

One (1) hourly data of variables such as 10 m wind speed (u_{10}), sea surface temperature (SST) and 2 m air temperature obtained from ERA5 Reanalysis over a 84 year (1940-2023) period were used to statistically evaluate the performance of thirteen (13) proposed predictive equations and some existing equations to predict wind friction velocity (u*) at omu creek, Mahin in Ilaje Local Government Area, Ondo State, Southwestern Nigeria. Results showed that Equation (9), u* = a + b(u) + c(Tr) + d(Tm) performed best in predicting u*. The frequency of the wind flow characteristics has been investigated in the location. Results showed that the transitional flow prevailed in the location. Also, investigation on the temporal trends in the wind flow characteristics showed that transition flow exhibited an inclining and the strongest trend of 0.0556% yr^{-1} throughout the study period. The aerodynamically smooth flow and the fully rough flow exhibited declining trends of −0.0495% yr^{-1} and −0.006% yr^{-1} respectively. Lastly, Equation (9) is tested in near and far waters. Findings showed that the formula performed best in Bijimi. This is attributed to the nearness of the location to omu creek than the rest locations. The formula showed the worst performance in Bakingil, Cameroon.

Keywords

Model, ERA5 Reanalysis, Prediction, Estimate, Annual, Seasonal, Monthly

1. Introduction

Heat, mass, and momentum are all exchanged between the ocean and the

atmosphere. The ocean's involvement in Earth's climate and its variability over both short and long timescales is defined by these air-sea interactions, which together make up the ocean's surface energy and water budgets. Their expertise is crucial for comprehending and simulating a number of physical processes involving different atmospheric and marine motion scales at appropriate geographical and temporal ranges. In numerical prediction, flux-related near-surface meteorological variables (wind speed, sea and air temperatures, and humidity) are frequently used to evaluate air-sea fluxes from bulk flux parameterization. For many years, the objective of research on air-sea interactions has been the creation of precise flux parameterizations (NEMO System Team) (https://doi.org/10.25424/cmcc/bulk_formulas_nemo_report).

In addition to having typically different temperatures, the air and the sea surface also have distinct specific humidity levels in the atmospheric layer and the atmospheric surface layer, respectively, which vary with height. A buoyant flux linked to sensible and latent heat transfers is ensured under these circumstances, which modifies the turbulent structure in the marine layer and alters the physical processes of the air-sea interaction.

During hurricane Sally, Hsu (2022) proposed formulations for the wind-stress from deep to shallow water by employing buoy 42,040 in the deep sea and buoy 42,012 in the shallow water. According to Andreas et al. (2012), u* can be expressed in terms of the 10-m neutral wind. In addition to processed (pre-calculated fluxes) datasets gathered on towers, ships, and other aircraft, their linear formulation of u* as a function of 10-m neutral wind is based on datasets from nine aircrafts. Vickers et al. (2015) proposed a formulation for the u* that is directly dependent on wind speed and bulk stability, which are two essential mean flow properties known to affect turbulence strength and momentum transfer. Their calculations showed good agreement with the bulk flux scheme of the Coupled Ocean-Atmosphere Response Experiment (COARE). A straightforward equation of u* as the product of the mean wind speed and mean bulk stability was developed by Vickers et al. (2015). They compared the u* predictions to aircraft data from the Greenland Flow Distortion Experiment (GFDEX; Petersen and Renfrew, 2009), observations from the Fronts and Atlantic Storm Track Experiment (FASTEX; Persson et al., 2005), and data from offshore platform towers from the Humidity Exchange over the sea (HEXOS; DeCosmo, 1991). Andreas et al. (2012, 2015) recently conducted an analysis on these three datasets. The basic formula to forecast the u* was fed values for the measurement height, mean wind speed, virtual potential temperature, and sea surface temperature. They found that the observed u* variance, which can be described by the simple formulation, varies greatly: 83% for FASTEX, 88% for GFDEX, and 92% for HEXOS. The absence of weak wind data, where the observed fluxes are least clear, contributes to these high R^2 values. For FASTEX, GFDEX, and HEXOS, the average u* values are 0.51 m/s, 0.75 m/s, and 0.48 m/s, respectively. Furthermore, due to the high wind speeds, the stability correction is negligible and the stability function's uncertainty becomes

less significant. For FASTEX, GFDEX, and HEXOS, the nondimensional slopes derived from linear regression are 1.13, 0.87, and 1.16, correspondingly. For FASTEX, GFDEX, and HEXOS, the corresponding mean biases in u* (the mean predicted value minus the mean observed) are −0.03, 0.02, and −0.07 m/s. For FASTEX, GFDEX, and HEXOS, the corresponding mean relative biases in u* (the mean formulated value minus the mean observed normalized by the mean) are −6%, 2%, and −15%. During the passage of six hurricanes over the wind seas with $u_{10} > 9$ m/s, three National Data Buoy Center (NDBC) buoys were used to measure wind speed at 10 m, significant wave height, Hs, and peak wave period simultaneously. The overwater u* was predicted by Shen et al. (2019), using the overwater downwind turbulence intensity. Based on wind-current interaction method data, they established that the proposed u* formula is valid up to u_{10} of 56 m/s during Super Typhoon Megi, 2010. Takagaki et al. (2016) proposed u* using a strong relationship between the inverse wave age and the equilibrium range constant. Their results imply that, in oceans under tropical cyclones, u* can be calculated only from wave data at very high wind speeds. A technique for the autonomous retrieval of the turbulent stress (or wind u*) from cross-polarized Sentinel-1 IW-mode SAR images was developed by Ermakova et al. (2023). This algorithm can be used for a variety of wind conditions, including hurricanes. Their results were found to be quite consistent when compared to the H14E and MS1A algorithms. Figueroa-Espinoza et al. (2022) provided a straightforward formula for estimating u*, which is subsequently verified using information from six separate studies conducted in coastal areas. The findings demonstrated that u* can be evaluated from 2D measurements with small root mean squared errors ($0.06 < \text{RMSE} < 0.097$) and high correlation coefficients ($0.77 < r^2 < 0.95$), thereby reducing the sensitivity to wind direction or atmospheric stability. Gao et al. (2021) examined the fluctuation of u* with u_{10} for wind speeds less than 17 m/s, using turbulent wind speed data from 11 airplane experiments. They noticed that as u_{10} increased, u* also increased. Using u_{10} of less than 16 m/s during two typhoons, Typhoon Hagupit and Typhoon Chanthu, off the coast of the South China Sea, Zhang et al. (2021) also made similar observations. This was further supported by Liu et al.'s (2012) research.

Fang et al. (2020) examined the changes in u* with wind speed and height in moderate (greater than or equal to 9 m/s) to strong onshore wind conditions. They observed that changes in u* with wind speed are influenced by wind direction. Under heavy onshore wind circumstances, a leveling out or reduction in u* occurs at a crucial wind speed of 20 m/s.

A flow is considered aerodynamically smooth when the Reynolds number (Re) is less than 0.13, and this value often corresponds to winds over the sea surface that are less than or equal to 2 - 3 m/s (Fairall et al., 1996). Andreas et al. (2012) stated that a flow is considered aerodynamically rough when $\text{Re} \geq 2.5$, and that this value typically corresponds to winds over the sea surface exceeding 9 m/s. Additionally, $u^* = 0.0583u_{10} - 0.243$ for entirely rough flow. In-between the fully

rough flow and aerodynamically smooth flow lies the transitional flow. Johnson et al. (1998) stated that the categorization of flow regimes into aerodynamically smooth flow, transition flow and fully rough flow over the sea is reliant on a roughness Reynolds number, in which the roughness length is replaced by the Charnock value. Smooth flow is typically associated with older, more established waves, while rough flow is associated with younger, developing waves.

Little or no work has been reported on the prediction of u* in the Niger Delta region in Nigeria, particularly over Omu creek, Mahin. Furthermore, the characterization of wind flow characteristics over the location has not received any attention till date. However, they are very significant in coastal management and maritime works.

The objectives of this work are to: 1) propose a formulation for the numerical prediction of u* as a function of the wind velocity at a height of 10 meters and the air-sea temperature difference; 2) investigate the performance of the proposed formula over near and far waters; and 3) characterize the flow characteristics in the study location using the Kraus and Businger's (1994) flow regime classification.

This paper is organized as follows: A thorough explanation of the field data collection process in relation to the verification of the satellite data utilized for this study is provided in Section 2. The approaches or parameterizations used in the air-sea interaction problem for the estimation of u* in the research location are presented in Section 3. Section 4 discusses the results; Section 5 provides a summary of the work completed and the conclusions.

1.1. Study Area

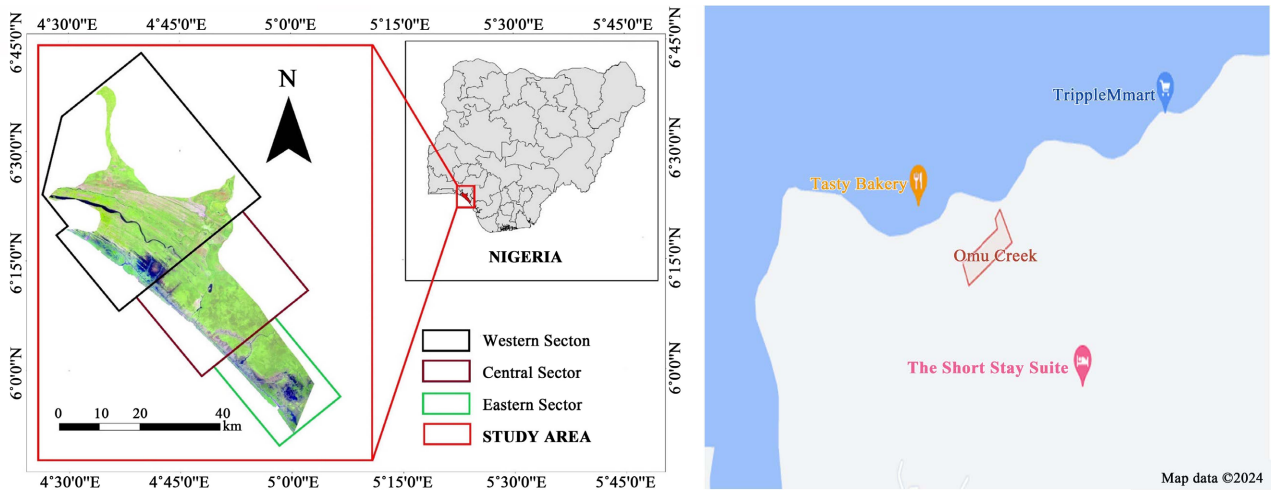

(a) (b)

Figure 1. (a) The Mahin mud coast of Ilaje, Nigeria extracted from Landsat imagery (Daramola et al., 2022). (b) Map of Omu creek in the mud coast. Map data ©2024.

The research area, Omu Creek (4.75E, 6.25N), is situated in the Niger Delta region of Nigeria, more precisely in Mahin, Ilaje Ese Odo, Ondo state. It is embedded in the 75-kilometer-long Mahin transgressive mud coast, which is located

in the Gulf of Guinea between the western and eastern ends of the Niger Delta (**Figure 1(a)** and **Figure 1(b)**). It stops at the mouth of the Benin River on the northwest edge of the Niger Delta. This is the point on Nigeria's coastline when it turns from east-west to southeast-northwest (Daramola et al., 2022). The creek is close to the settlements of Ito-Omu and Badore. It is a naturally occurring stream that is important to the local economy and ecology. The creek is home to a variety of aquatic animals and is encircled by mangrove trees. Access to fishing grounds and other resources is made possible by it, making it a crucial transportation route for the nearby towns. Omu Creek has suffered from pollution and environmental deterioration, primarily as a result of nearby oil prospecting and other human activity. The ecosystem of the creek is being restored and preserved for next generations. The creek finally empties into the Atlantic Ocean after passing through portions of the states of Rivers and Bayelsa. The creek's abundant biodiversity, which includes a wide variety of fish species, crabs, and other aquatic life, is well-known. In addition to offering crucial habitat for wildlife, the nearby mangrove forests provide as a natural defense against erosion and storm surges. Additionally, the creek helps the nearby towns by supplying fish for food and revenue from fishing operations. Nevertheless, pollution and environmental deterioration have an impact on Omu Creek, as they do on numerous other Niger Delta waterways. The ecology of the creek has deteriorated as a result of deforestation, rubbish dumping, and oil spills. To address these problems and improve Omu Creek's health, efforts are being made. In order to restore mangroves, clean up the stream, and encourage sustainable fishing methods, local communities, government organizations, and environmental organizations are collaborating. All things considered, Omu Creek is an important natural resource in the Niger Delta, and the local populations that rely on it as well as the environment need it to be preserved and restored. The tropical climate of the area usually has an impact on the weather and climate in the study region. Its climate is classified as tropical wet and dry, or savanna (Aw). The district experiences an annual temperature of 28.76˚C (83.77˚F), which is −0.7% colder than the average for Nigeria. The region experiences 194.21 wet days (53.21% of the time) and 132.4 millimeters (5.21 inches) of precipitation on average each year. There are distinct wet and dry seasons, with April through October usually seeing the most rainfall. Humidity can still be rather high during the dry season, which typically lasts from November to March. Source: ChatGPT 3.5, also known as the Chat Generative Pre-trained Transformer.

2. Data Source, Validation and Error Analysis

2.1. The "Sea Truth" Data Campaigns

The Omu Creek Air-Sea Interaction Experiment began with onshore wind-wave parameter measurements at Omu Creek, Mahin coast (4.75E, 6.25N), during the following dates: February 3-17, 2023, and April 1-11, 2023. The experiment's objectives were to collect data on peak wave period (Tp), 10 m wind speed (u_{10}), and 2 m wind speed (u_2) in order to compute u* in the field. The study site is located

11 meters above mean sea level (MSL). A 30 m high meteorological tower, located 1 km from shore and with an upstream fetch of 10 - 15 km, was chosen for this experiment. It was situated in a 90 degree sector with an upstream water depth of 5 - 20 m, in approximately 4 m of water. A Gill Wind Master Pro ultrasonic anemometer (UA) and a Campbell RM Young 05106 wind monitor were utilized and suspended from the tower at 2 m and 10 m heights respectively. The tower stands 3 meters above mean sea level. The mean wind speed was derived from the cup anemometer at 2 m and 10 m. The peak wave period was derived from the spectral analysis of the time series of pixel intensities and filtering to avoid noise. Data were logged as 30-min time series and sampled at 20 Hz. Data were remotely relayed by radio from the tripod to a nearby shore station.

2.2. Computation of u* and Data Validation

Direct observations of u* are usually not available. Field data from u_2, u_{10}, and Tp collected between February 3-17, 2023, and April 1-11, 2023, were used in the computation. By using a logarithmic profile in the air, the relation for u_{10} is obtained (Bye and Wolff, 2008),

$$u_{10} = u_2 - \frac{u_*}{k}\ln\left(\frac{c_p^2}{2gz_{10}}\right) \tag{1}$$

where $c_p = gT_P/2pi$ is the peak wave speed, u_2 is the surface, 2 m wind speed, $z_{10} = 10$ m, $g = 9.8$ m/s, $pi = 3.142$ and κ is the von Kármán constant. Here, $\kappa = 0.4$ and u* was computed from the above relation. A validation experiment was conducted for the ERA5 reanalysis, u*. One (1) hourly averaged field data of u_2, u_{10} and T_p were collected at the study site for the periods indicated above and inputted into the above equation for the calculation of u*. The ERA5 Reanalysis data of u* for the same location and for Feb 3rd-17th, 2023 were sourced from https://cds.climate.copernicus.eu/user. Excellent comparisons between the computed u* and u* obtained from ERA5 are shown in **Figure 2(a)**. The values of r, RMSE, and MBE are 0.9995, 0.0022, and −7.5E−05 m/s, respectively.

Again, the computation of u* is repeated for the field data of u_2, u_{10} and T_p gathered during April 1st-11th, 2023. The computed u* compared well with u* from ERA5 Reanalysis. The time series with the scatter plots are presented in **Figure 2(b)**. The values of r, RMSE, and MBE are respectively 0.9996, 0.002, and 7.99E−05 m/s. The negative bias indicated that the ERA5 Reanalysis data under predicted the observed data and vice versa for the positive bias. The ERA5 reanalysis data for u* generally agreed with the observational u*, suggesting that the reanalysis data can be trusted to accurately model u* in the research location.

3. Predicting u*

Seventeen (17) equations have been used in this study to evaluate u*. Thirteen (13) were proposed in this work and the rest four (4) were existing models by some authors. These models are presented in **Table 1**.

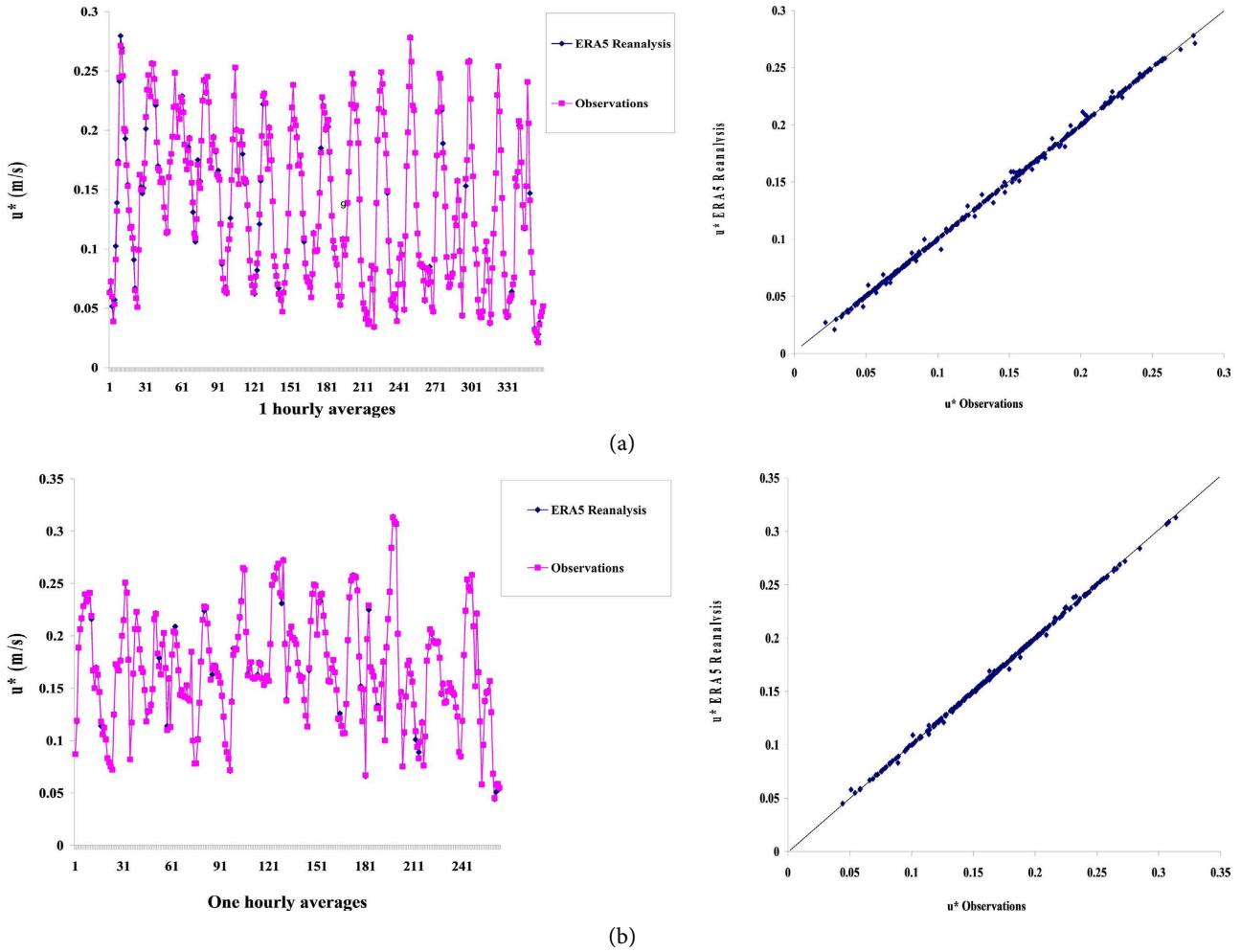

Figure 2. (a) Time series comparisons from Feb 3rd-17th, 2023 and (b) from April 1st-11th, 2023 for u* between ERA5 Reanalysis and observation.

Table 1. Predictive equations used for this study.

Model	Form
1	$u^* = a + b(u) + c(u^2) + d(u^3) + e(u^4)$
2	$u^* = a + b(Tr/Tm)$
3	$u^* = a + b(Tr) + c(Tm)$
4	$u^* = a + b(Tair) + c(SST)$
5	$u^* = a + b(Tair - SST)$
6	$u^* = a + b(u) + cln(Tr/Tm)$
7	$u^* = a + b(u/Tr/Tm)$
8	$u^* = a + bln(Tr/Tm)$
9	$u^* = a + b(u) + c(Tr) + d(Tm)$
10	$u^* = a + bln(Tair - SST)^2$
11	$u^* = a + b(u) + c(Tair) + d(SST)$

Continued

12	$u^* = a + b\ln(u)$
13	$u^* = a + b\exp(Tr/Tm)$
Yelland and Taylor, 1996	$u^* = 0.11038 + 0.00217u + 0.00278u^2 - 0.000044u^3$
Foreman and Emeis, 2010	$u^* = 0.0019u^2 + 0.033(u - 8) + 0.3$
Fang et al., 2018	$u^* = 0.0283u + 0.00513$
Andreas et al., 2012	$u^* = 0.0015u^2 + 0.0099u + 0.062$

For the air-sea temperature analysis, the temperature ratio: $T_r = T_a/T_w$ and the mean temperature: $T_m = (T_a + T_w)/2$, where T_a and T_w are respectively the 2 m air temperature and SST.

The aforementioned formulations provide values for the years as well as the dry season (November-March) and wet season (April-October). The three established statistical techniques which are r, RMSE, and MBE, have been used to test the equations.

4. Results

Table 2. (a)-(d): Summary of the regression constants, r, MBE and RMSE for u* between ERA5 Reanalysis and estimations for the years, seasons and months. The regression constants and the computed r, MBE and RMSE for other authors are also included.

(a) Annual

Model	a	b	c	d	e	r	MBE	RMSE
1	0.1123	−0.0548	0.0059	0.0111	−0.0017	0.9313	0.0002	0.0156
2	−0.4896	17.8902				0.7508	−2.50E−06	0.0283
3	−0.2152	0.7588	−0.0135			0.8298	1.94E−05	0.0238
4	0.4918	0.0202	−0.0318			0.82471	−8.60E−05	0.024
5	0.1695	0.0212				0.7726	6.62E−07	0.0272
6	0.7578	0.0469	0.22			0.9347	−9.00E−07	0.0152
7	−0.019	0.0022				0.8674	−1.60E−05	0.0213
8	2.2191	0.6209				0.7496	1.12E−06	0.0283
9	−0.1784	0.0417	0.3412	−0.0041		0.9583	−1.00E−04	0.0122
10	0.1924	−0.0391				0.8134	−6.50E−07	0.0249
11	0.1368	0.0421	0.0099	−0.0132		0.9576	−0.0001	0.0123
12	0.0224	0.1286				0.8802	1.18E−07	0.0203
13	−17.757	17.2785				0.7509	2.34E−05	0.0283
Yelland and Taylor, 1996	0.11038	0.00217	0.00278	4.4E−05		0.9261	−0.005	0.0338
Foreman and Emeis, 2010	0.0019	0.033	0.3			0.9181	−0.0013	0.02
Fang et al., 2018	0.0283	0.00513				0.9129	−0.0558	0.0618
Andreas et al., 2012	0.0015	0.0099	0.062			0.9219	−0.0326	0.0458

Continued

(b) Dry Season								
Model	a	b	c	d	e	r	MBE	RMSE
1	0.0507	0.1047	−0.1138	0.0449	−0.0049	0.8761	0.0002	0.0178
2	−0.5704	20.4021				0.7359	3.03E−06	0.0249
3	−0.4262	0.3586	0.0076			0.8097	−8.64E−06	0.0216
4	−0.0823	0.0164	−0.0083			0.8107	6.11E−05	0.0216
5	0.1495	0.0162				0.8062	−3.40E−07	0.0218
6	1.4099	0.0388	0.4069			0.9269	5.96E−07	0.0138
7	0.0035	0.0017				0.7909	−2.10E−05	0.0226
8	2.4857	0.6985				0.7403	9.95E−07	0.0248
9	−0.321	0.0357	0.2109	0.0058		0.9541	−1.20E−05	0.011
10	0.1733	−0.0309				0.7428	−2.50E−06	0.0247
11	−0.1187	0.0356	0.0104	−0.0042		0.9544	−0.0001	0.011
12	0.0366	0.1064				0.8186	−3.20E−07	0.0212
13	−20.271	19.7123				0.7357	3.54E−06	0.0249
Yelland and Taylor, 1996	0.11038	0.00217	0.00278	4.4E−05		0.8657	0.0018	0.0297
Foreman and Emeis, 2010	0.0019	0.033	0.3			0.8528	0.0027	0.0204
Fang et al., 2018								
Andreas et al., 2012	0.0283	0.00513				0.8468	−0.0502	0.0557
(c) Wet Season								
Model	a	b	c	d	e	r	MBE	RMSE
1	0.1436	−0.1337	0.0615	−0.0032	−0.0005	0.9557	1.49E−05	0.0134
2	−0.4944	17.9492				0.7532	3.36E−06	0.03
3	−0.3862	0.9032	−0.0119			0.8745	−8.50E−05	0.0221
4	0.4541	0.0265	−0.0361			0.8696	−2.20E−05	0.0225
5	0.1921	0.0286				0.8346	−4.20E−08	0.0251
6	0.3657	0.0546	0.1088			0.948	1.22E−06	0.0145
7	−0.0319	0.0024				0.9184	4.04E−06	0.018
8	2.2255	0.6237				0.7485	−2.30E−07	0.0302
9	−0.2273	0.0443	0.3356	−0.0022		0.9676	5.19E−05	0.0115
10	0.2038	−0.0439				0.8594	7.41E−06	0.0233
11	0.0805	0.0449	0.0108	−0.012		0.9669	2.55E−05	0.0116
12	0.0138	0.1413				0.9162	1.68E−07	0.0183
13	−17.818	17.3342				0.7533	−1.60E−05	0.03
Yelland and Taylor, 1996	0.11038	0.00217	0.00278	4.4E−05		0.951	−0.0099	0.0365

Continued

Foreman and Emeis, 2010	0.0019	0.033	0.3			0.9474	−0.0041	0.0198
Fang et al., 2018	0.0283	0.00513				0.9438	−0.0598	0.0658
Andreas et al., 2012	0.0015	0.0099	0.062			0.9496	−0.0374	0.0504
				(d) Monthly				
Model	a	b	c	d	e	r	MBE	RMSE
1	−0.2578	0.4242	−0.1453	0.0149	0.0005	0.9972	−2.80E−06	0.0018
2	−0.2966	12.3033				0.7539	−2.10E−06	0.0154
3	−0.4065	0.9347	−0.0124			0.8069	−8.80E−05	0.0138
4	0.4688	0.0268	−0.0371			0.8066	−4.70E−05	0.0139
5	0.2012	0.0375				0.6919	−1.30E−06	0.0169
6	0.1478	0.0553	0.0448			0.9966	1.75E−06	0.0019
7	0.0043	1.3155				0.9861	1.65E−07	0.0039
8	1.5704	0.4283				0.7515	3.04E−07	0.0155
9	0.1065	0.0586	−0.0799	−0.0016		0.9981	−6.30E−05	0.0014
10	0.2102	−0.0718				0.8728	4.29E−06	0.0114
11	0.0317	0.0585	−0.0036	0.0018		0.9981	0.0001	0.0014
12	0.0363	0.1222				0.9897	−4.40E−07	0.0034
13	−12.171	11.8813				0.754	4.79E−05	0.0154
Yelland and Taylor, 1996	0.11038	0.00217	0.00278	4.4E−05		0.9957	−0.005	0.0181
Foreman and Emeis, 2010	0.0019	0.033	0.3			0.9955	0.1266	0.0068
Fang et al., 2018	0.0283	0.00513				0.995	−0.0558	0.0571
Andreas et al., 2012	0.0015	0.0099	0.062			0.9958	−0.0326	0.0365

Presented in Tables 2(a)-(d) is a summary of the regression constants and other statistical tests to evaluate the performance of the proposed equations for predicting u* on an annual, seasonal and monthly basis over the study area. For the annual prediction in Table 2(a), model 9 exhibits higher r and lower RMSE values than the other equations and best predicts u*. The r and RMSE are respectively 0.9583, and 0.0122. A MBE of −1E−04 showed that model 9 under predicted u*. Models 2, 5, 8 and 13 with respective r values of 0.7508, 0.7726, 0.7496 and 0.7509 and RMSE values of 0.0283, 0.0272, 0.0283 and 0.0283 respectively, least predict u*. Model 2 with MBE of −2.5E−06 underestimates u*, while models 5, 8 and 13 with respective MBE values of 6.62E−07, 1.12E−06 and 2.34E−05 over evaluate u*. Models 1, 3, 4, 6, 7, 10, 11 and 12 exhibited respective r values of 0.9313, 0.8298, 0.82471, 0.9347, 0.8674, 0.8134, 0.9576 and 0.8802. The MBE values are respectively 0.0002, 1.94E−05, −8.6E−05, −9E−07, −1.6E−05, −6.5E−07, −0.0001 and 1.18E−07, while the RMSE values are respectively 0.0156, 0.0238, 0.024, 0.0152, 0.0213, 0.0249, 0.0123, 0.0203. u* is underestimated in models 4, 6, 7, 10

and 11, while it is over predicted in models 1, 3 and 12. Regarding the 13 models proposed in this study, model 9 having the least RMSE of 0.0122 is to be preferred for short-term prediction of u*, while model 12, having the least MBE of 1.18E−07, is to be preferred for long-term prediction of u*.

Also in assessing the performance of the equations proposed by some authors, the model proposed by Yelland and Taylor (1996), whose r and RMSE are respectively 0.9261 and 0.0338 performed better than the rest three models. Although the parameterization of Foreman and Emeis (2010), exhibited a lower RMSE of 0.0200 but it has a lower r value of 0.9181. The authors' formulation with MBE values of −0.0050, −0.0013, −0.0558 and −0.0326 all under evaluated u*.

For the seasonal evaluation in tables 2b and c, the r has a seasonal dependence with r being higher in the wet than during the dry season, which implies that the equations generally perform better during the wet season. During the wet season, model 9 has higher r and lower RMSE values than the other equations and therefore, best predicts u*. The r and RMSE are respectively 0.9676 and 0.0115. A MBE of 5.19E−05 showed that model 9 over predicted u*. The u* is least evaluated in models 2, 8 and 13. The r values are respectively 0.7532, 0.7485 and 0.7533, while the RMSE values are respectively 0.03, 0.0302 and 0.03. The u* is over predicted in models 1, 2, 6, 7, 9, 10, 11 and 12, while it is under evaluated in models 3, 4, 5, 8 and 13. Model 9 having the least RMSE of 0.0115 is to be preferred for short-term prediction of u*, while model 5, having the least MBE of −4.2E−08, is to be preferred for long-term prediction of u*. The formulation of Yelland and Taylor (1996), whose r and RMSE are respectively 0.9510 and 0.0365 performed better than the equations from the rest authors. However, the formulation of Foreman and Emeis (2010), showed a lower RMSE of 0.0198 but it exhibited a lower r value of 0.9474. The negative MBE values showed that u* is under predicted in the predictions from the authors.

For the monthly evaluation in **Table 2(d)**, it is obvious that r is higher in most of the equations (except in models 3, 4 and 5) when monthly estimates are used than when the actual annual one hourly data are used, therefore u* generally yields better performance with monthly values. Again, model 9 has higher r (0.9981), with lower MBE (−6.3E−05) and RMSE (0.0014) values than the other equations proposed in this study and therefore, best predicts u*. Model 11 also showed an excellent prediction of u* but it has a larger MBE (0.0001) than that of model 9. The u* is least estimated in models 2, 5, 8 and 13. The r values are respectively 0.7539, 0.6919, 0.7515 and 0.7540, while the RMSE values are respectively 0.0154, 0.0169, 0.0155 and 0.0154. u* is under evaluated in models 1 - 5, 9 and 12, while it is over evaluated in models 6, 7, 8, 10, 11 and 13. Models 9 and 11, having the least RMSE values of 0.0014 and are to be preferred for short-term prediction of u*, while model 7, having the least MBE of 1.65E−07, is to be preferred for long-term prediction of u*. Again, the formulation of Yelland and Taylor (1996), whose r, MBE and RMSE values are respectively 0.9957, −0.0050 and 0.0181 performed better than the equations from the rest authors. Although the formulation of

Andreas et al. (2012) exhibited a higher r value of 0.9958, but the values of MBE (-0.0326) and RMSE (0.0365) are larger than that of Yelland and Taylor (1996). The u* is only over predicted (MBE = 0.1266) in the formulation of Foreman and Emeis (2010), while it is underestimated in the equations from the rest authors.

The u* relationship for Yelland and Taylor (1996) has the disadvantage that it must not be extrapolated above 26 m/s. It would predict decreasing wind stress values for wind speeds above 30 m/s.

To construct the dependencies for u* in the range specified in a study by Ermakova et al. (2023), the parameterizations of u* on u from Foreman and Emeis (2010) was used. Different parameterizations give different results, which indicate an uncertainty in determining the value of u*. It is obviously related to the choice of a specific parameterization, and thus the quality of the results greatly depends on which particular parameterization is to be chosen from the currently existing ones.

The u* from Fang et al. (2018) is only applicable for the lower wind speed range when the wind speed is less than 8 m/s.

Andreas et al. (2012) proposed a formulation for the u* in terms of the 10-m neutral wind. This approach reduces the self-correlation between u* and 10-m neutral wind. Their linear formulation of u* as a function of the 10-m neutral wind is based on nine aircraft datasets used in a study with the addition of processed (precalculated fluxes) datasets collected on towers, ships, and other aircraft. While there is no roughness length in their formulation, the method still relies on Monin-Obukhov similarity theory because the stability function is a function of the Obukhov length. The formulation must be solved iteratively because u* is required to estimate 10-m neutral wind, which is used to estimate u*, and so on. The formulation of Andreas et al. (2012) has the desirable property that the 10-m neutral equivalent drag coefficient naturally rolls off at high wind speed and asymptotically approaches a constant value of $3.4*10^{-3}$.

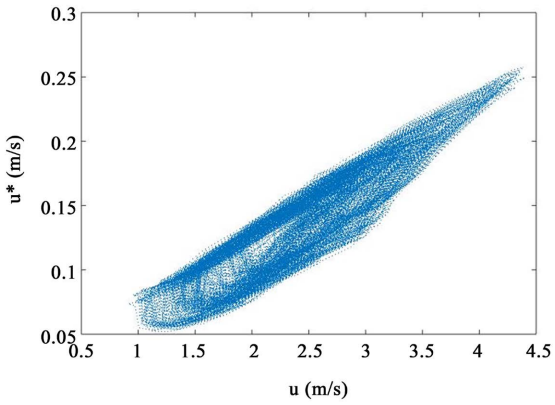

Figure 3. The variations in u* with u_{10}.

The variations in u* with u_{10} in **Figure 3**, are studied under low to moderate (0.0036 - 7.1619 m/s) onshore wind conditions. u* increases with increasing wind

speed. This agrees with the findings of Fang et al. (2018). However, in literatures, a leveling-off or decrease in u* with increasing wind speed is found under strong wind conditions especially at wind speeds higher than 22 m/s. u* increases with increasing wind speed at a similar growth rate to that of previously published results.

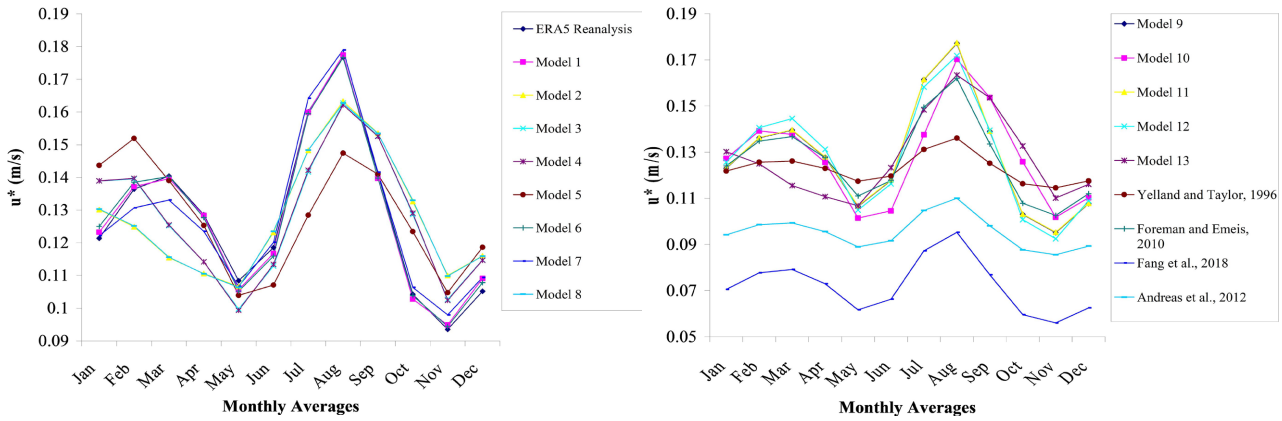

(a) (b)

Figure 4. Monthly variation of u* for the equations proposed in this study and for the authors.

Figure 4(a) and **Figure 4(b)** present the monthly variation of u*. For all the equations, the u* is lowest in November (0.0560 m/s - 0.1145 m/s) and largest in August (0.0952 m/s - 0.1790 m/s). For all the monthly values of u*, the mean u* ranged between 0.0721 m/s and 0.1280 m/s, the standard deviation ranged between 0.0064 m/s and 0.0245 m/s and the percentage coefficient of variation ranged between 5.2060% and 19.1362%. In individual months, the percentage coefficient of variation is the least in August (4.7% - 14.01%) and in most cases, the largest in November (5.58% - 26.2%).

4.1. Characterization of Flow Regimes at Omu Creek

Table 3. Percentage frequencies of flow regimes over the study region for the year, seasons and months.

	Aerodynamically Smooth Flow	Transition Flow	Fully Rough Flow
Annual	43.41	54.35	2.18
Dry	47.99	51.32	0.64
Wet	40.16	56.52	3.27
Jan	46.67	52.82	0.46
Feb	37.03	61.49	1.43
Mar	32.98	65.67	1.30
Apr	41.45	57.64	0.85
May	56.22	43.32	0.42

Continued

Jun	48.99	49.98	0.97
Jul	23.82	69.82	6.30
Aug	15.89	73.27	10.78
Sep	35.56	61.28	3.08
Oct	59.36	40.28	0.30
Nov	66.10	33.84	0.01
Dec	56.79	43.11	0.05

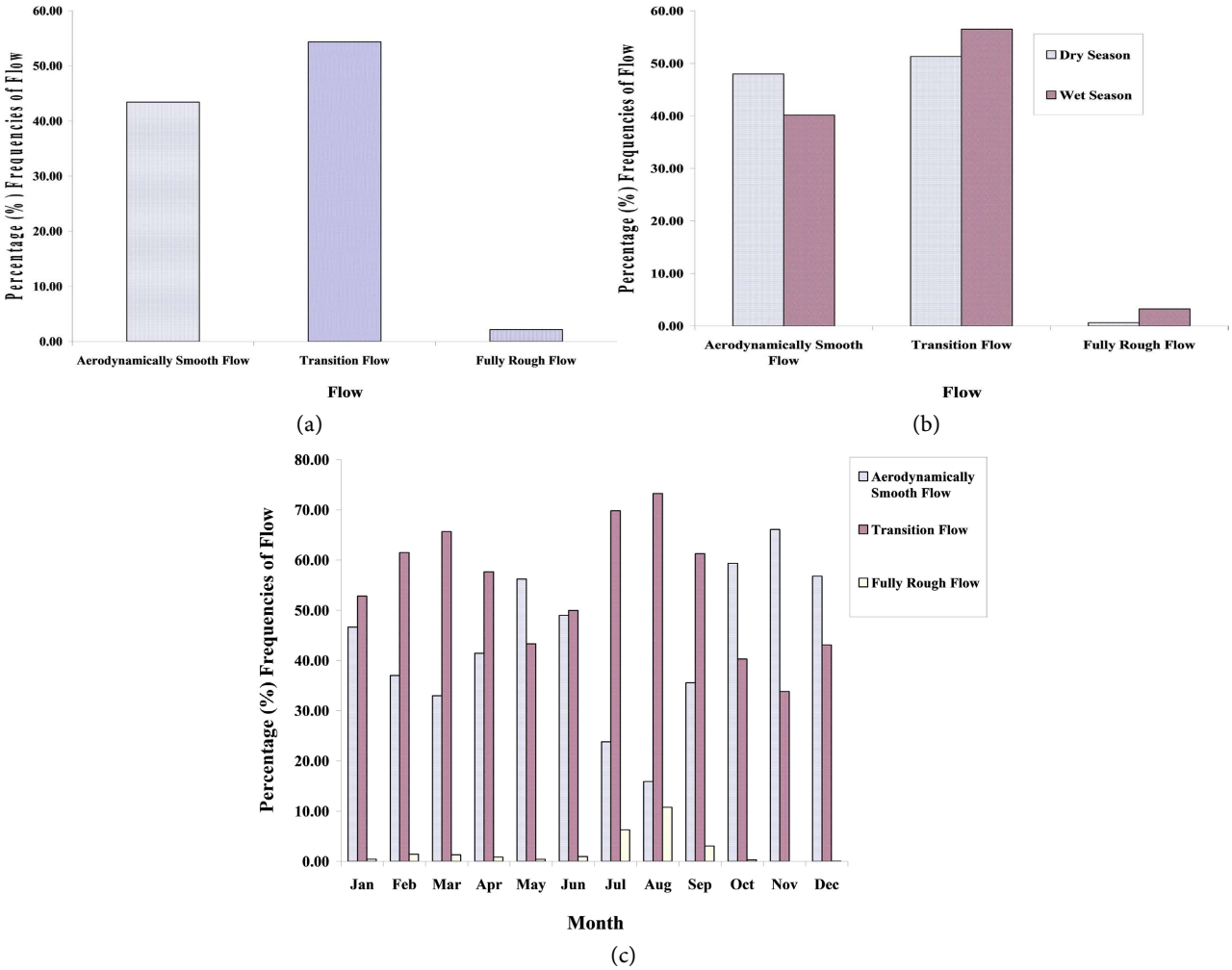

Figure 5. Bar plots for the (a) annual, (b) seasonal and (c) monthly percentage frequencies of flow regime over the study region.

The u* data in the study location has been subdivided into classes of different flow regimes as shown in **Table 3**, using the method of Kraus and Businger (1994). They are aerodynamically smooth flow: (u* < 0.11 m/s), transition flow: (0.11 m/s < u* < 0.265 m/s) and Fully rough flow: (0.265 m/s < u*).

The annual, seasonal and monthly mean cumulative percentages of frequency for the different flow regimes using u* are as shown in **Figures 5(a)-(c)**. For the

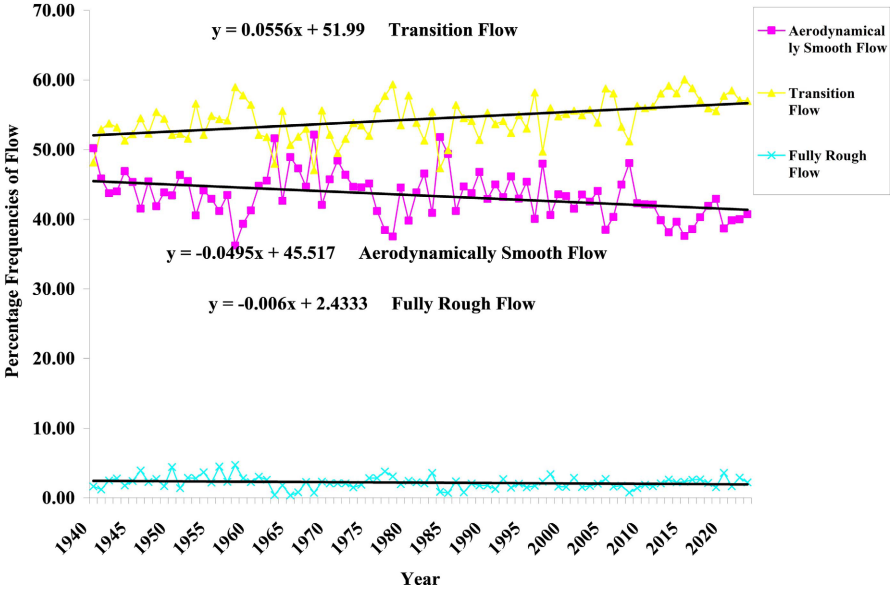

Figure 6. Trends in the annual averaged percentage frequency flow regimes in the study location from 1940 to 2023.

annual mean characterization (Figure 5(a)), the transition flow has the highest percentage occurrence of 54.35% all through the study location. The occurrence of the aerodynamically smooth flow is relatively smaller (43.41%). Hardly is the flow condition in the location a fully rough one (2.18%).

For the seasonal flow characteristics presented in Figure 5(b), the transition flow has the largest percentage frequencies of 51.32% and 56.52% both during dry and wet seasons. The aerodynamically smooth flow showed lower occurrences of 47.99% and 40.16% respectively during dry and wet seasons. For both seasons, hardly is the flow condition fully rough. The occurrence is 0.64% during the dry season and 3.27% during the wet season. In all, the sea is rougher during the wet season.

The monthly mean characterization in Figure 5(c), suggests that the transition flow has higher occurrence in all months than the aerodynamically smooth flow except in the months of May and October through December with respective frequencies of 43.32%, 40.28%, 33.84% and 43.11%. The occurrence of the transition flow is largest in August (73.27%) and least in November (33.84%). The occurrence of the aerodynamically smooth flow is largest in November (66.10%) and least in August (15.89%), implying that the sea is smoothest in November and roughest in August. Higher occurrences of the fully rough flow showed in July (6.30%) and August (10.78%). It occurred least in November (0.01%).

Temporal trends in the percentage frequencies of flow regimes over the study location are shown in Figure 6. The transition flow exhibited an inclining and the strongest trend of 0.0556% yr^{-1} throughout the study period. Peak occurrence in transition flow occurred in 2015 (60.07%) and the lowest occurrence (47.04%) occurred in 1968. The aerodynamically smooth flow exhibited a declining trend of -0.0495% yr^{-1} all through the years. It has the largest occurrence (52.15 %) in 1968

and the least (36.21%) in 1958. The fully rough flow exhibited a declining and the weakest trend of −0.006% yr^{-1} all through the years. The occurrence (4.69%) peaked in 1958 and least (0.35 %) in 1965. In general, the fully rough flow occurred at higher frequencies in 1946 (3.92%), 1950 (4.41%), 1954 (3.68%), 1956 (4.47%), 1958 (4.69%), 1961 (3.03%), 1977 (3.78%), 1978 (3.07%), 1983 (3.57%), 1998 (3.40%) and 2020 (3.57%). The aerodynamically smooth flow occurred at higher frequencies in 1940 (50.19%), 1963 (51.61%), 1968 (52.15%) and 1984 (51.79%).

4.2. Applying Model 9 to Near and Far Waters

Model 9, which performed best in the prediction of u* in omu creek, has been tested in Bijimi in ilaje, Ondo state, Nigeria (4.75E 6N), which is a near location to omu creek and in far locations such as Bakingil in Cameroon (9E 4N), isioke in Rivers state, Nigeria (7.5E 4.5N), Etukegbene in Bayelsa state, Nigeria (6E 4.5N), Okusikiri in Rivers state, Nigeria (7E 4.5N) and Eduwini in Bayelsa state, Nigeria (5.5E 5N). The summary of the r, MBE and RMSE for u* (1940-2023) between ERA5 Reanalysis and the u* obtained, using model 9 for the individual locations is displayed in Table 4.

Table 4. Summary of the r, MBE and RMSE for u* between ERA5 Reanalysis and estimations for the years.

Location	r	MBE	RMSE
Bakingil	0.8483	−0.0696	0.0708
Isioke	0.9263	−0.0859	0.0871
Etukegbene	0.9216	−0.0907	0.0922
Okusikiri	0.9103	−0.0900	0.0920
Eduwini	0.9249	−0.0959	0.0970
Bijimi	0.9615	−0.0572	0.0589

From the table, Bijimi has a higher r (0.9615) and lower MBE (−0.0572) and RMSE (0.0589) values than those of the other locations therefore, model 9 worked best in Bijimi. This is attributed to the nearness of the location to omu creek than the rest locations. A MBE of −0.0572 showed that model 9 under evaluated u* from ERA5 Reanalysis over the location. Model 9 performed least in Bakingil since it has the least value of r = 0.8483. The MBE and RMSE values are respectively −0.0696 and 0.0708. For the individual locations, negative MBE values implied that model 9 under evaluated u* from ERA5 Reanalysis.

5. Conclusion

This work has statistically evaluated the performance of eighteen (18) predictive equations for evaluating u* the study area. Observational data of u* compared well with the ERA5 Reanalysis data. The predictive equations were evaluated on an annual, seasonal and monthly basis. Results showed that in all cases, model 9,

performed best in predicting u* in the study location. All the equations generally performed better in the wet than in the dry season.

For the monthly prediction, u* generally yields better performance with monthly values. The formulation proposed by Yelland and Taylor (1996) in general, performed better than the rest three existing models. The u* increases with increasing wind speed. This agrees with the findings of Fang et al. (2018). It is found to be lowest in November (0.0560 m/s - 0.1145 m/s) and largest in August (0.0952 m/s - 0.1790 m/s).

The transition flow has the highest percentage occurrence of 54.35% all through the study location. It showed the largest percentage frequencies of 51.32% and 56.52% both during dry and wet seasons. The aerodynamically smooth flow showed lower occurrences of 47.99% and 40.16% respectively during dry and wet seasons, thereby suggesting that the sea is rougher during the wet season. The monthly mean characterization suggests that the transition flow has higher occurrence in all months than the aerodynamically smooth flow except in the months of May and October through December with respective frequencies of 43.32%, 40.28%, 33.84% and 43.11%. The occurrence of the transition flow is largest in August (73.27%) and least in November (33.84%). The occurrence of the aerodynamically smooth flow is the largest in November (66.10%) and the least in August (15.89%), implying that the sea is smoothest in November and roughest in August. Higher occurrences of the fully rough flow showed in July (6.30%) and August (10.78%). It occurred least in November (0.01%).

The transition flow exhibited an inclining and the strongest trend of 0.0556% yr^{-1} throughout the study period. The aerodynamically smooth flow exhibited a declining trend of −0.0495% yr^{-1} all through the years. The fully rough flow exhibited a declining and the weakest trend of −0.006% yr^{-1} all through the years.

Lastly, model 9 is tested in near and far waters. Findings showed that the formulation performed best in Bijimi. This is attributed to the nearness of the location to Omu creek than the rest locations. The model showed the worst performance in Bakingil, Cameroon.

For future research, the role of u* can be investigated in extreme weather events such as hurricanes and typhoons and in climate model predictions. Impacts of ocean surface currents can be studied on u* and its implications for ocean-atmosphere exchange processes. Also, the unique challenges and opportunities for researches on u* can be made in polar regions. By exploring these avenues, researchers can advance our understanding of u* over the sea and improve its parameterization in numerical models.

Code Availability

The Matlab codes used in the methodology of this work may be found at https://www.mathworks.com/products/matlab.html.

Data Availability

The two principal sources of data used for this work are the *in situ* data collected

at the study site and ERA5 Reanalysis data, sourced from https://cds.climate.copernicus.eu/user.

Author Contributions

The conceptualization, methodology, software, validation, data analysis, investigation, resources, data curation, writing—review and editing, visualization, supervision and project administration for this work were all jointly provided by all the authors to this paper.

Acknowledgements

I wish to acknowledge the inestimable contributions of Prof Okogbue Emmanuel Chilekwu of the Department of Meteorology and Climate Science, Federal University of Technology Akure, Ondo State, Nigeria, in the suggestion of suitable statistical methods used for the error analysis in this work. Your contributions are well acknowledged.

Conflicts of Interest

There are no competing interests to declare for this work.

References

Andreas, E. L., Mahrt, L., & Vickers, D. (2012). A New Drag Relation for Aerodynamically Rough Flow over the Ocean. *Journal of the Atmospheric Sciences, 69,* 2520-2537. https://doi.org/10.1175/jas-d-11-0312.1

Andreas, E. L., Mahrt, L., & Vickers, D. (2015). An Improved Bulk Air-Sea Surface Flux Algorithm, Including Spray-Mediated Transfer. *Quarterly Journal of the Royal Meteorological Society, 141,* 642-654. https://doi.org/10.1002/qj.2424

Bye, J. A. T., & Wolff, J. (2008). Charnock Dynamics: A Model for the Velocity Structure in the Wave Boundary Layer of the Air-Sea Interface. *Ocean Dynamics, 58,* 31-42. https://doi.org/10.1007/s10236-007-0130-5

Daramola, S., Li, H., Omonigbehin, O., Faruwa, A., & Gong, Z. (2022). Recent Retreat and Flood Dominant Areas along the Muddy Mahin Coastline of Ilaje, Nigeria. *Regional Studies in Marine Science, 52,* Article ID: 102272. https://doi.org/10.1016/j.rsma.2022.102272

DeCosmo, J. (1991). *Air-Sea Exchange of Momentum, Heat and Water Vapor over White-Cap Sea States.* Ph.D. Thesis, University of Washington.

Ermakova, O., Rusakov, N., Poplavsky, E., Sergeev, D., & Troitskaya, Y. (2023). Friction Velocity and Aerodynamic Drag Coefficient Retrieval from Sentinel-1 IW Cross-Polarization C-SAR Images under Hurricane Conditions. *Remote Sensing, 15,* Article 1985. https://doi.org/10.3390/rs15081985

Fairall, C. W., Grachev, A. A., Bedard, A. J., & Nishiyama, R. T. (1996). *Wind, Wave, Stress and Surface Roughness Relationships from Turbulence Measurements Made on R/P Flip in the Scope Experiment.* A Report for the DoD ASAP Program Environmental Sensing Program Element (P.ETL.2090).

Fang, P., Jiang, W., Tang, J., Lei, X., & Tan, J. (2020). Variations in Friction Velocity with Wind Speed and Height for Moderate-To-Strong Onshore Winds Based on Measure-

ments from a Coastal Tower. *Journal of Applied Meteorology and Climatology, 59,* 637-650. https://doi.org/10.1175/jamc-d-18-0327.1

Fang, P., Zhao, B., Zeng, Z., Yu, H., Lei, X., & Tan, J. (2018). Effects of Wind Direction on Variations in Friction Velocity with Wind Speed under Conditions of Strong Onshore Wind. *Journal of Geophysical Research: Atmospheres, 123,* 7340-7353. https://doi.org/10.1029/2017jd028010

Figueroa-Espinoza, B., Sánchez-Mejía, Z., Uuh-Sonda, J. M., Salles, P., Méndez-Barroso, L., & Gutiérrez-Jurado, H. A. (2022). Friction Velocity Estimation Using a 2D Sonic Anemometer in Coastal Zones. *Atmósfera, 35,* 673-685. https://doi.org/10.20937/atm.52960

Foreman, R. J., & Emeis, S. (2010). Revisiting the Definition of the Drag Coefficient in the Marine Atmospheric Boundary Layer. *Journal of Physical Oceanography, 40,* 2325-2332. https://doi.org/10.1175/2010jpo4420.1

Gao, Z., Zhou, S., Zhang, J., Zeng, Z., & Bi, X. (2021). Parameterization of Sea Surface Drag Coefficient for All Wind Regimes Using 11 Aircraft Eddy-Covariance Measurement Databases. *Atmosphere, 12,* Article 1485. https://doi.org/10.3390/atmos12111485

Hsu, S. (2022). Wind-stress Variations from Deep to Shallow Water during Hurricanes for Air-Sea-Land Interaction Applications. *Advances in Environmental and Engineering Research, 3,* 1-1. https://doi.org/10.21926/aeer.2201006

Johnson, H. K., Højstrup, J., Vested, H. J., & Larsen, S. E. (1998). On the Dependence of Sea Surface Roughness on Wind Waves. *Journal of Physical Oceanography, 28,* 1702-1716. https://doi.org/10.1175/1520-0485(1998)028<1702:otdoss>2.0.co;2

Kraus, E. B., & Businger, J. A. (1994). *Atmosphere-Ocean Interaction* (2nd ed., p. 362). Oxford University Press.

Liu, B., Guan, C., & Xie, L. (2012). The Wave State and Sea Spray Related Parameterization of Wind Stress Applicable from Low to Extreme Winds. *Journal of Geophysical Research: Oceans, 117,* C00J22. https://doi.org/10.1029/2011jc007786

NEMO System Team. *NEMO Ocean Engine: Bulk Formulations in NEMOv.4: Algorithms Review and Sea Surface Temperature Response in ORCA025 Case Study.* https://doi.org/10.25424/cmcc/bulk_formulas_nemo_report

Persson, P. O. G., Hare, J. E., Fairall, C. W., & Otto, W. D. (2005). Air-Sea Interaction Processes in Warm and Cold Sectors of Extratropical Cyclonic Storms Observed during Fastex. *Quarterly Journal of the Royal Meteorological Society, 131,* 877-912. https://doi.org/10.1256/qj.03.181

Petersen, G. N., & Renfrew, I. A. (2009). Aircraft-Based Observations of Air-Sea Fluxes over Denmark Strait and the Irminger Sea during High Wind Speed Conditions. *Quarterly Journal of the Royal Meteorological Society, 135,* 2030-2045. https://doi.org/10.1002/qj.355

Shen, H., He, Y., & Hsu, S. A. (2019). Estimating Downwind Turbulence Intensity Using Wind and Wave Measurements during Hurricanes. *Applied Ocean Research, 88,* 71-75. https://doi.org/10.1016/j.apor.2019.04.011

Takagaki, N., Komori, S., & Suzuki, N. (2016). Estimation of Friction Velocity from the Wind-Wave Spectrum at Extremely High Wind Speeds. *IOP Conference Series: Earth and Environmental Science, 35,* Article ID: 012009. https://doi.org/10.1088/1755-1315/35/1/012009

Vickers, D., Mahrt, L., & Andreas, E. L. (2015). Formulation of the Sea Surface Friction Velocity in Terms of the Mean Wind and Bulk Stability. *Journal of Applied Meteorology and Climatology, 54,* 691-703. https://doi.org/10.1175/jamc-d-14-0099.1

Yelland, M., & Taylor, P. K. (1996). Wind Stress Measurements from the Open Ocean. *Journal of Physical Oceanography, 26,* 541-558.

https://doi.org/10.1175/1520-0485(1996)026<0541:wsmfto>2.0.co;2

Zhang, X., Bi, X., Gao, Z., Liu, C., Peng, W., Zeng, Z., Yang, N., & Li, Y. (2021). Parameterizations of Drag Coefficient and Aerodynamic Roughness Length Using the Turbulence Data Collected during Typhoons Hagupit and Chanthu. *Journal of Tropical Oceanography, 40,* 1-6. https://doi.org/10.11978/2020047